Synthesis, thermal properties, vibrational spectra and computational studies of Trioctylmethylammonium bis(trifluoromethylsulfonyl)imide ionic liquid

Mohammed Amin Assenine, Boumediene Haddad, Annalisa Paolone, Silvia Antonia Brandán, Mimanne Goussem, Didier Villemin, Mostefa Boumediene, Mustapha Rahmouni, Serge Bresson

Synthesis, thermal properties, vibrational spectra and computational studies of Trioctylmethylammonium bis(trifluoromethylsulfonyl)imide ionic liquid

Mohammed Amin Assenine [1], Boumediene Haddad [2,3,4,*], Annalisa Paolone [5], Silvia Antonia Brandán [6], Mimanne Goussem[1], Didier Villemin [3], Mostefa Boumediene [2], Mustapha Rahmouni [4], Serge Bresson[7].

[1] Université Djillali Liabes, BP 89, 22000 Sidi-Bel-Abbes, Algeria

[2] Department of Chemistry, Faculty of Sciences, Dr Moulay Tahar University of Saïda, Algeria

[3] LCMT, ENSICAEN, UMR 6507 CNRS, University of Caen, 6 bd Ml Juin, 14050 Caen, France

[4] Synthesis and Catalysis Laboratory LSCT, Tiaret University, Tiaret, Algeria

[5] CNR-ISC, U.O.S. La Sapienza, Piazzale A. Moro 5, 00185 Roma, Italy

[6] Cátedra de Química General, Instituto de Química Inorgánica, Facultad de Bioquímica. Química y Farmacia, Universidad Nacional de Tucumán, Ayacucho 471, (4000) San Miguel de Tucumán, Tucumán, Argentina.

[7] Laboratoire de Physique des Systèmes Complexes, Université Picardie Jules Verne, 33 rue St Leu 80039 Amiens cedex, France.

* Corresponding author: Haddad Boumediene, Department of Chemistry, Faculty of Sciences, Dr Moulay Tahar University of Saïda, Algeria.

E-mail: haddadboumediene@yahoo.com Tel.: +00213676802567

ABSTRACT

In this work, Aliquat 336 ([Aliquat$^+$]) based ionic liquids containing the fluorinated anion bis(trifluoromethylsulfonyl)imide [NTf$_2^-$] is successfully prepared by the anionic exchange replacement of the chloride anion. The reaction of lithium bis(trifluoromethylsulfonyl)imide with *N*-Methyl-*N,N,N*-trioctylammonium chloride ([N$_{1,8,8,8}$][Cl] in water leads to the corresponding IL, namely ([Aliquat$^+$][NTf$_2^-$]). The obtained ionic liquid was characterized by using infrared and Raman spectra and its structure was confirmed by ^{1}H-NMR, ^{13}C-NMR, and ^{19}F-NMR. The thermal properties were investigated by two complementary thermal analysis techniques: TGA and DTA. A hexadentate coordination mode between cation-anion was predicted by atoms in molecules (AIM) studies for the [Aliquat$^+$][NTf$_2^-$] IL by using B3LYP/6-31G* calculations where three O atoms of the anion are linked to six H atoms of cation by S-O$\cdots$H interactions. Changes in the bond orders of S and O atoms of the cation support such observations. The predicted cation-anion distances are in the range 2.30-2.60 Å. The harmonic force fields of cation and anion were calculated and the complete assignments were performed for both species while the most important bands observed in the infrared and Raman spectra of the IL were assigned. In addition, the scaled force constants of cation and anion of the IL are also reported.

1. INTRODUCTION:

Investigations on ionic liquids have increased remarkably in recent times due to their versatile physical-chemical properties which include very low vapor pressure, liquid state at room temperature, non-flammability, high solubility power, good solvent capacity and their potential as designer solvents for catalytic, chemical applications and in processes relating to transport and storage of energy [1-9]. Ionic liquids (ILs) such as, imidazolium, pyridinium, ammonium, pyrrolidinium were investigated as potential candidates for many applications [10-13], e.g. as efficient corrosion inhibitors for several metals and alloys [14]. In particular, the tetraalkylammonium salts $[C_iC_jC_kC_lN]^+$ (with i,j,k,l referring to number of carbon atoms in alkyl chains) have evidenced good corrosion inhibition properties compared with their heterocyclic analogues [15]. In this sense, Aliquat 336, also known as ($[N_{1,8,8,8}][Cl]$) or *N*-Methyl-*N,N,N*-trioctylammonium or tricaprylmethylammonium, is a quaternary ammonium salt that exhibits quite unusual and distinctive properties with major applications, such as phase transfer catalysis, lubrication, metal extraction, and removal of metals from hydrochloric acid solutions [16-21]. Besides, Aliquat 336 is more stable against air and moisture attack than other cationic ligands and it is easy to handle [22]. A great advantage is that the synthesis reactions of Aliquat ionic liquids are more environmentally benign and friendly [23]. Hence, the preparation and properties of this family are a rapidly growing area of research interest [24-26]. Mikkola et al. have reported that the use of Aliquat 336 in many chemical reactions could be limited due to the strong coordination effect of the chloride anion [27]. Hence, the cation-anion interaction in ionic liquids is a key factor determining the physico-chemical properties of ILs [28,29]. The design of new ILs with anions different from Cl$^-$ could provide interesting physico-chemical properties and, for these reasons, the knowledge about the synthesis, the thermal and vibrational properties and interaction between coupled cation-anion in these ILs are important subjects. Studies on vibrational properties, intermolecular vibrations, molecular conformations, and hydrogen-bonded interactions are of great interest in ionic liquids [30-34]. Experimental techniques such as, infrared (IR) and Raman spectroscopies have provided new insights on ionic interactions and the resulting liquid structure in ionic liquids [35-38]. The combination of synthesis and spectroscopic properties with quantum chemistry calculations allows the elucidation of intra- and inter-ionic interactions in new ionic liquids [35-38]. Structural and vibrational studies of quaternary

ammonium prepared from mono-, bi-, tri-, and tetra-alkylammonium cations combined with several anions have been reported by different authors [36, 39-49] but, so far, the complete assignments of FTIR and Raman spectra of Aliquat 336 have not been reported, yet. The present work focuses on the synthesis, characterization of the thermal and vibrational properties of a Aliquat based ionic liquid, namely Aliquat (bis(trifluoromethylsulfonyl) Imide) ([Aliquat$^+$][NTf$_2^-$]). This Aliquat ionic liquid has been synthesized and characterized by infrared and Raman spectroscopies being its structure confirmed by using ^{1}H, ^{13}C and ^{19}F-NMR spectroscopies. The interpretation of vibrational spectra performed using infrared (FTIR/ATR) and Raman spectroscopy and a detailed DFT investigation of ionic liquid was also performed. In this work, the cation and anion of the Aliquat based ionic liquid were also structural and vibrationally characterized.

2. Experimental

2.1. Materials and methods

The chemicals used in this study are *N*-Methyl-*N,N,N*-trioctylammonium chloride (> 99%) and lithium bis(trifluoromethylsulfonyl)imide (99%). They were purchased from Aldrich and used as received. Deionized H$_2$O was obtained with a Millipore ion-exchange resin deionizer.

2.2. General procedure for the synthesis of Aliquat 336 IL

Firstly, the quaternary ammonium salt ([Aliquat$^+$][Cl$^-$]) is obtained commercially and was used as received. The reaction of lithium bis(trifluoromethylsulfonyl)imide with *N*-Methyl-*N,N,N*-trioctylammonium chloride in water leads to the corresponding IL namely ([Aliquat$^+$] [NTf$_2^-$]). In detail, the synthesis of ([Aliquat$^+$][NTf$_2^-$]) can be described as follows [50]. Lithium bis(trifluoromethylsulfonyl)imide (2.87 g, 10 mmol) dissolved in 10 mL of deionized water was added in a flask containing *N*-Methyl-*N,N,N*-trioctylammonium chloride (4.32 g, 10mmol) dissolved in 5 mL of deionized water. The mixture consisted of two separate phases: the ionic liquid at the bottom and an aqueous solution at the top. The former was separated from the latter by centrifugation (2000 rpm) for 600 seconds. After isolation, the obtained [Aliquat$^+$][NTf$_2^-$] was washed with distilled water several times to eliminate LiCl residues and was dried in phosphorus pentoxide, P$_2$O$_5$, to remove residual water. The obtained product is yellowish viscous liquids (Yield: 65%). The removal of the chloride ions was followed by testing the aqueous solution by chloride precipitation using AgNO$_3$. The obtained compounds

were investigated by NMR in order to probe the desired structure (see next sub-section).The structure of the ionic liquid prepared and studied in the present work is shown in **Scheme 1**.
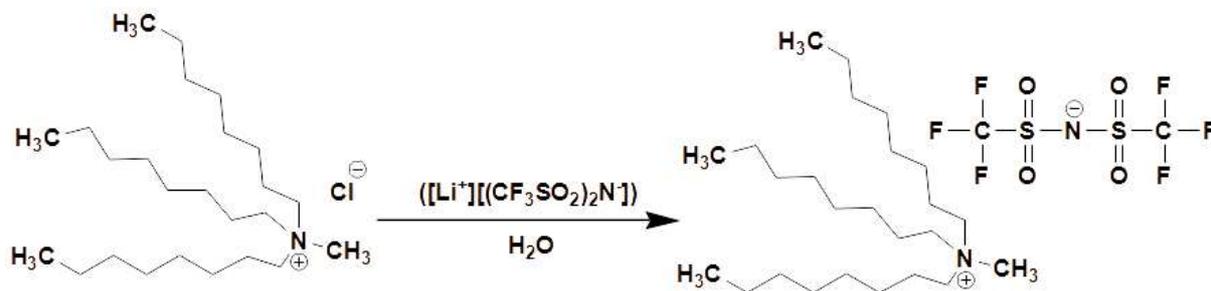
Scheme 1: The synthesis process of ([Aliquat$^+$][NTf$_2^-$]).

2.3. NMR analysis

The structure and purity of the synthesized ionic liquid was confirmed by NMR analysis: ^{1}H-NMR (400 MHz) and ^{13}C-NMR (100 MHz) spectra were recorded on a DRX 400 MHz spectrometer (400 MHz). The chemical shifts (δ) are given in ppm and referred to the internal solvent signal namely tetramethylsilane (TMS) and trichlorofluoromethane (CFCl$_3$).

2.4. Thermal analysis

Concomitant measurements of thermogravimetry (TGA) and differential thermal analysis (DTA) were performed by means of a Setaram Setsys Evolution 1200 TG System, with a fixed temperature rate of 5°C/min, in an argon flux of 60 ml/min. For each sample, an initial mass of ~20 mg was used.

2.5. Vibrational spectroscopy

2.5.1. FTIR/ATR measurements

The FTIR/ATR measurements were acquired on a Bruker Vertex II-70RAM Spectrometer (Bruker Analytical, Madison, WI) operating with a Golden Gate diamond ATR accessory TM (Specac Ltd, Slough, United Kingdom). The FTIR/ATR spectra were collected with 1 cm^{-1} nominal resolution by co-adding 64 scans for each spectrum in the range 600-4000 cm^{-1}. The OPUS Software 6.0 for Windows was used for the management of the instrument.

2.5.2. FT-RAMAN measurements

FT-Raman spectra were acquired on a Vertex 70-RAM II Bruker FT-Raman spectrometer. This instrument is equipped with a Nd:YAG laser (yttrium aluminium garnet crystal doped with triply ionized neodymium) with a wavelength of 1064 nm and a maximum power of 1.5 W. The measurement accessory is pre-aligned: only the Z-axis of the scattered light is adjusted to set the sample in the appropriate position regarding the local measurement point. The RAM II spectrometer is equipped with a liquid nitrogen cooled Ge detector. FT-Raman spectra were collected with 1 cm^{-1} resolution by co-adding 128 scans for each spectrum at room temperature in the range 45-4000cm^{-1}. The OPUS 6.0 software was used for the spectral acquisition, manipulation and transformation. These both measurements FTIR/ATR and FT-RAMAN were performed in the Walloon Agricultural Research Center (Craw) Belgium.

3. Computational

The *GaussView* program was used to model the [Aliquat$^+$][NTf$_2$$^-$] ionic liquid and its [Aliquat$^+$] cationic and [NTf$_2$$^-$] anionic species [51] and, later the three structures were optimized in gas phase with the Revision A.02 of Gaussian 09 program [52] by using the functional hybrid B3LYP with the 6-31G* basis set [53,54]. The structures of cation and anion are shown in **Figure 1** while the corresponding [Aliquat$^+$][NTf$_2$$^-$] ionic liquid can be seen in **Figure 2**.

Figure 1. Structures of [Aliquat$^+$] cation and [NTf$_2$$^-$] anion species of [Aliquat$^+$][NTf$_2$$^-$] ionic liquid and atoms labelling.

Figure 2. Structure of [Aliquat$^+$][NTf$_2$$^-$] ionic liquid and atoms labelling.
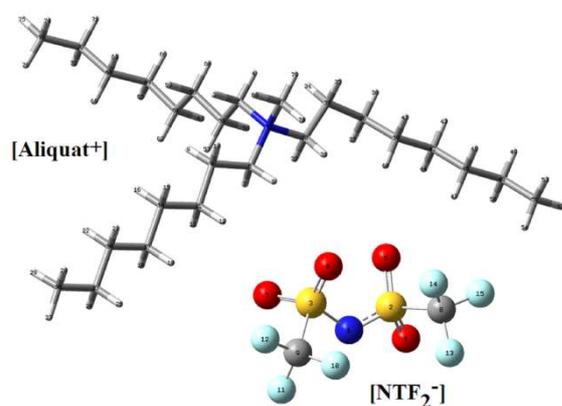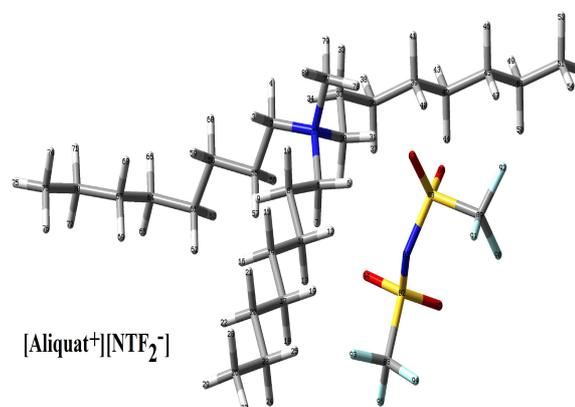
Natural bond orbital (NBO) and atoms in molecules (AIM) calculations were performed in order to investigate donor-acceptor energy interactions, atomic charges, molecular electrostatic potentials, bond orders, and topological properties of those three species at the same level of theory [55-58]. Then, the determinations of force fields of cation and anion

were carried out with the scaled quantum mechanical force field (SQMFF) methodology by using the normal internal coordinates, transferable scaling factors and the Version 7.0 of Molvib program [59-61] while the vibrational assignments for the ionic liquid were performed with the aid of *GaussView* program and, using a scale factor only for the vibration modes corresponding to higher wavenumbers [51]. Known equations were used to transform the Raman spectra predicted in activities for the three species to intensities [62,63]. On the other side, the gauge-including atomic orbital (GIAO) method was used to predict the ^{1}H and ^{13}C-NMR chemical shifts because it is a quantum mechanical technique for the calculation of magnetic properties of chemical systems [64]. Finally, the gap values together with interesting chemical potential (μ), electronegativity (χ), global hardness (η), global softness (S), global electrophilicity index (ω) and global nucleophilicity index (E) descriptors were calculated from their corresponding frontier orbitals [34,37,38].

4. Results and discussion

4.1. NMR results

In order to confirm the absence of significant impurities in the investigated IL, the ^{1}H, ^{13}C and ^{19}F-NMR spectroscopy was used to confirm the formation of the [Aliquat$^+$][NTf$_2^-$] IL by anionic exchange from [Aliquat$^+$][Cl$^-$]. The spectroscopic data are given below and the H and C atom labelling and the corresponding spectra are shown in **Figure 3** (A, B and C).

[Aliquat$^+$][NTf$_2^-$]:^{1}H-NMR (400 MHz, (CDCl$_3$) δ_H (ppm)= 3.11-3.15 (N$^+$–(CH$_2$)$_n$–, 6H), 2.96 (N$^+$-CH$_3$,3H), 1.58 (N$^+$–(CH$_2$)—(CH$_2$)–, 6H), 1.23-1.31 (–(CH$_2$)$_n$–, 30H), 0.83-086 (–(CH$_2$)$_n$—CH$_3$, *J=4 Hz*, 9H).^{13}**C-NMR**(100 MHz, (CDCl$_3$) δ_C (ppm)= 121.07(C$_{anion}$), 118.14 (C$_{anion}$), 61.62 (C7), 48.34 (C8), 31.60, 31.42 (C6), 28.79 (C5), 25.95 (C4), 22.49 (C3), 22.39 (C2), 13.86 (C1).^{19}**F-NMR**(100 MHz, CDCl$_3$) δ_F (ppm) =-78.82 ppm singulet.

As shown in **Figure 3** (A), the signals at δ =3.11-3.15 ppm were assigned to the methylene protons on the alkyl rings N$^+$–(CH$_2$)$_n$–. The signal at δ =2.96 ppm corresponding to the N$^+$-CH$_3$, thus, another three signals in the range of δ =1.58, broad at δ =1.23-1.31 ppm and δ =0.83-086 ppm were attributed to the methylene N$^+$–(CH$_2$)—(CH$_2$)– and –(CH$_2$)$_n$– groups in octyl chains and terminal methyl group –(CH$_2$)$_n$—CH$_3$ respectively.

F-NMR

-78.82

-61 -63 -65 -67 -69 -71 -73 -75 -77 -79 -81 -83 -85 -87 -89 -91 -93 -95 -97 -99
f1 (ppm)
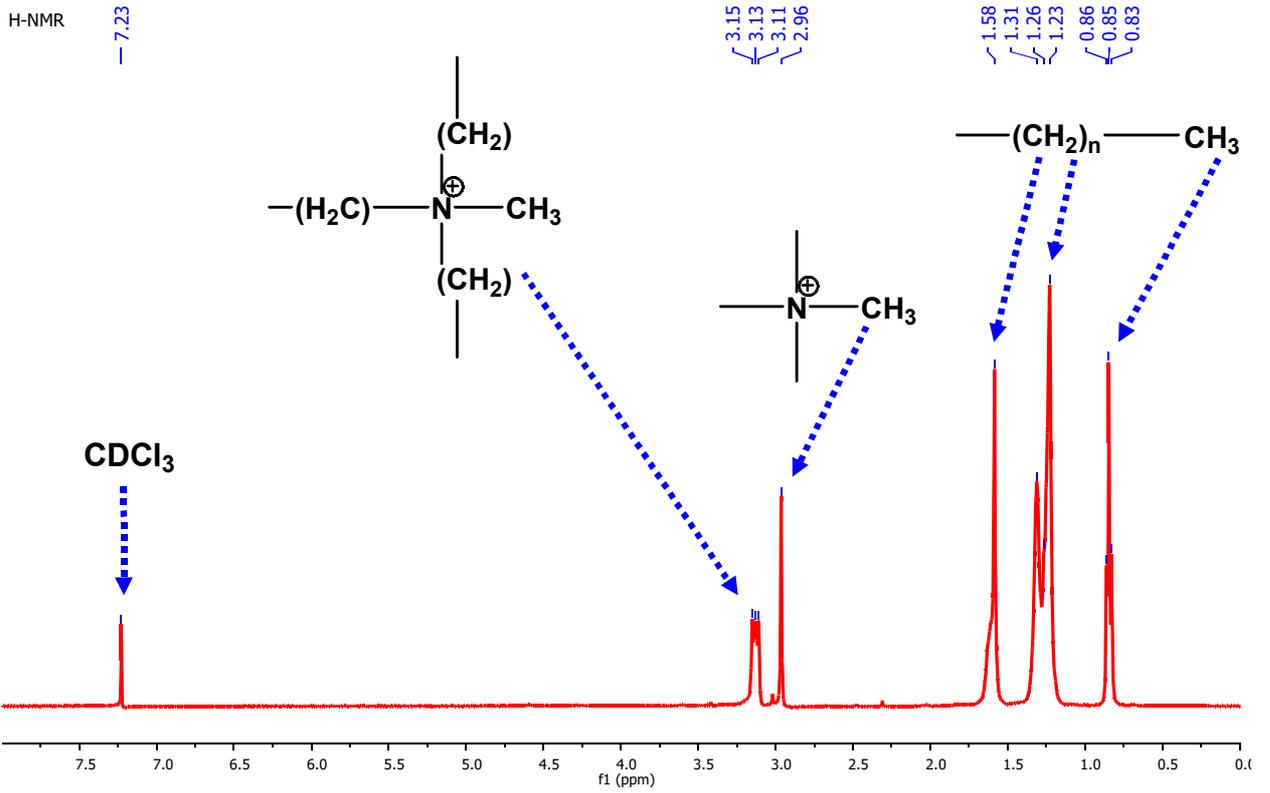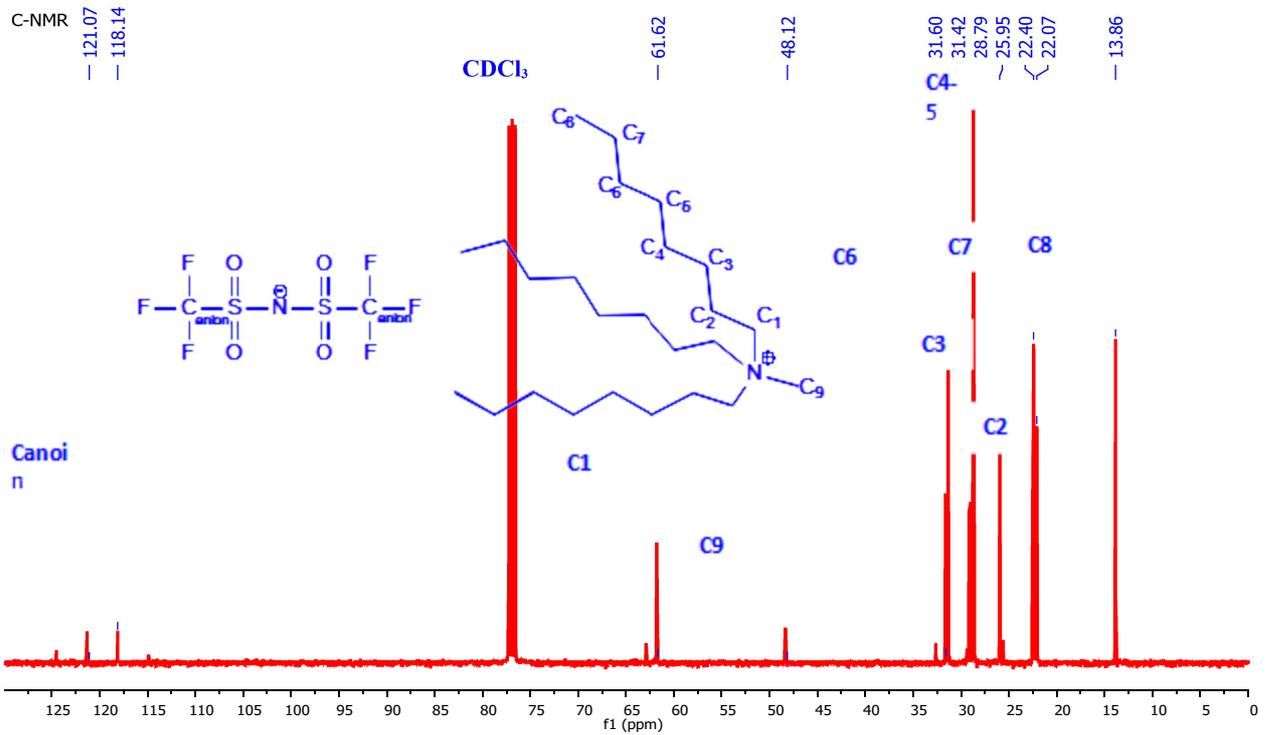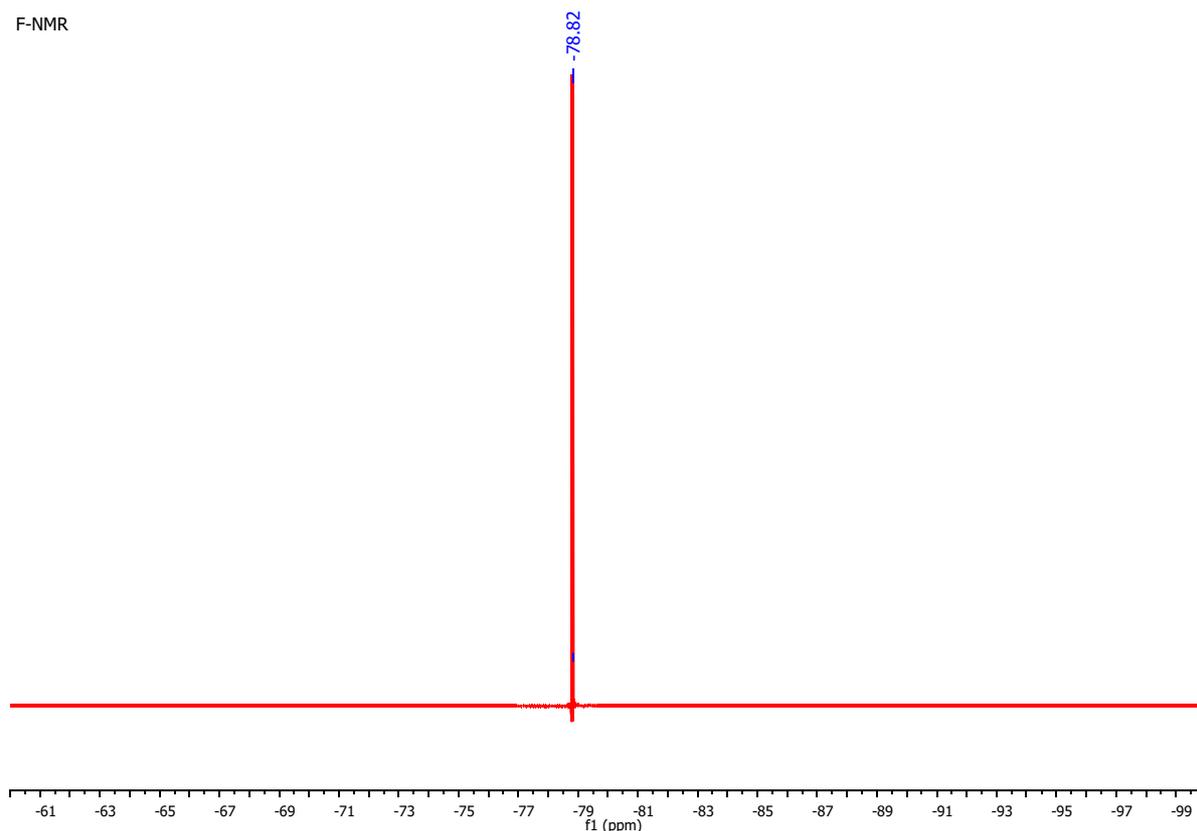
Figure 3. Hydrogen atom labeling and ^{1}H-NMR spectrum, carbon atom labeling and ^{13}C-NMR spectrum and ^{19}F-NMR spectrum of ([Aliquat$^+$][NTf$_2^-$]).

Moreover, the anionic exchange replacement of the chloride by bis(trifluoromethylsulfonyl)imide is demonstrated by the appearance of two new signals in the 13 C spectrum (**Figure 3 B**) as a doublet at δ = 121.07/118.14 ppm corresponding to the signature of the carbon of the [NTf$_2^-$] anion indicating the successful synthesis of [Aliquat$^+$][NTf$_2^-$]. Comparisons of predicted ^{1}H and ^{13}C-NMR chemical shifts by using the GIAO/B3LYP/6-31G* method for the [Aliquat$^+$][NTf$_2^-$] IL in gas phase by using the root-mean-square deviation (RMSD) values show a better correlation for the H nuclei (0.5 ppm) than the C atoms (20.3 ppm) [64]. The employed method and the gas medium justify such differences. Here, the IL calculations were not optimized in a solution.

4.2. Optimization geometries

The hybrid B3LYP/6-31G* method was used to optimize the ionic liquid couple due to the 95 atoms present in the structure; for comparison its cationic and anionic species were also optimized at the same level of theory. When the anion is optimized with C_{2V} symmetry by using the B3LYP/6-31G* method imaginary frequencies are obtained, while if this species is

optimized with C_I symmetry all positive frequencies are calculated when the 6-311++G** basis set is used. On the contrary, both cation and ionic liquid species are optimized with C_I symmetry and all positive frequencies are obtained by using the B3LYP/6-31G* basis set. Calculated total energies, dipole moments and volumes of cation, anion and [Aliquat$^+$][NTf$_2$$^-$] ionic liquid in gas phase by using the functional hybrid B3LYP method and the 6-31G* and 6-311++G** basis sets can be seen in **Table 1**. Comparing the properties for the anion with both methods it is observed that lower dipole moment and volume values are obtained with the higher size basis set.

Table 1. Calculated total energies (E), dipole moments (μ) and volumes (V) for cation, anion and [Aliquat$^+$][NTf$_2$$^-$] ionic liquid in gas phase by using the hybrid B3LYP/6-31G* Method.

Species	E (Hartrees)	μ (D)	V (Å^3)
B3LYP/6-31G* Method			
[NTf$_2$$^-$]$^{\#}$ (C_{2v})	-1827.0348	5.49	185.5
[Aliquat$^+$] (C_I)	-1039.7644	4.67	509.0
[Aliquat$^+$][NTf$_2$$^-$] ($C_I$)	-2867.0854	13.62	690.4
B3LYP/6-311++G** Method			
[NTf$_2$$^-$] ($C_I$)	-1827.6092	4.36	183.3

$^{\#}$Imaginary frequencies. The corresponding symmetries are indicated in parentheses

As expected due to its larger size, the [Aliquat$^+$][NTf$_2$$^-$] ionic couple presents higher dipole moment and volume. Regarding the dipole moment vectors for the three species in gas phase by using the two B3LYP/6-31G* and B3LYP/6-311++G** levels of theory, it is observed from **Figure S1** that orientations and directions of dipole moment vectors for the anionic and cationic species change notably in the ionic couple. Thus, in the anion the vector is located from centre of N atom in direction towards outside of two CF$_3$ groups while in the cationic species; the vector is located forming a certain angle in the direction of N1-CH$_3$ bond, as shown in Fig. S1. On the other hand, in the ionic liquid, the vector is practically parallel to N1-CH$_3$ bond in direction towards the large side chain. These results show that in the formation of ionic liquid the anion and the cation modify their dipole moment vector s.

Also other parameters are modified passing from the isolated ions to the ionic couple.In **Table 2** the calculated bond lengths and angles for anion, cation and ionic couple in the gas phase are summarized by using two levels of theory. The differences between cation and IL and between anion and IL are expressed by means of the root-mean-square deviation (RMSD) values.

Table 2. Comparison of calculated geometrical parameters for cation, anion and [Aliquat$^+$][NTf$_2$$^-$] ionic liquid in gas phase at different levels of theory.

	B3LYP/6-31G*[a]				
Bond lengths (Å)	[Aliquat⁺]	[Aliquat⁺][NTf₂⁻]	Bond angles (º)	[Aliquat⁺]	[Aliquat⁺][NTf₂⁻]
N1-C2 (R)	1.531	1.517	C2-N1-C5	111.6	111.5
N1-C5 (R)	1.536	1.539	C2-N1-C30	112.0	112.0
N1-C30 (R)	1.536	1.541	C5-N1-C30	106.4	107.2
N1-C77 (CH₃)	1.505	1.505	C2-N1-C77	107.9	108.8
RMSD		**0.008**			**1.1**
Bond lengths (Å)	[NTf₂⁻][#]	[Aliquat⁺][NTf₂⁻]	Bond angles (º)	[NTf₂⁻][#]	[Aliquat⁺][NTf₂⁻]
N81-S82	1.599	1.631	S82-N81-S83	125.9	122.3
N81-S83	1.614	1.605	O84-S82-O85	119.3	118.2
S82-O84	1.460	1.479	O86-S83-O87	118.2	117.3
S82-O85	1.463	1.464	N81-S82-O84	108.7	111.6
S83-O86	1.463	1.474	N81-S83-O87	113.1	108.1
S83-O87	1.462	1.477	N81-S82-C88	96.0	96.6
S82-C88	1.897	1.868	N81-S83-C89	103.9	104.6
S83-C89	1.891	1.869			
RMSD		**0.020**			**2.7**

[a]This work, [#]From B3LYP/6-311++G** method; RMSD values in letter bold.

The higher differences in the RMSD values are observed in bond lengths and angles of the anion with values of 0.020 Å for lengths and 2.7 º for angles while for the cation the variations for bond lengths and angles are ~ 0.008 Å and 1.1 º, respectively. This way, the anion undergoes important changes in the formation of IL. These observations could be justified due to the long side chains that probably stabilize anion and cation in the IL.

4.3. Atomic charges, molecular electrostatic potentials and bond orders

The slight modifications observed in the geometrical parameters of anion suggest that this species play a important role in the formation of IL and in their properties and, for this reason, atomic charges, molecular electrostatic potentials and bond orders are investigated for cation and anion by separate and, then, for the IL. Hence, in Table S1 we presented atomic Merz-Kollman (MK), Mulliken and natural population (NPA) charges, molecular electrostatic potentials and bond orders only for the atoms corresponding to cation and anion of those three species in gas phase. Note that for the cation only the three types of charges on N1 atoms are compared in Table S1 with that corresponding to IL while in Figure S2 we presented the variations in MK, Mulliken and NPA charges observed only on the atoms corresponding to anion and to IL. Analyzing the three charges on the N1 atoms of cation it is observed that only the MK charge on N1 of cation (0.133 a.u.) is different from that observed in the IL (-0.376 a.u.) while the Mulliken and NPA charges are practically the same in both species. Hence, the

values of the MK charges on N1 atoms demonstrate differences between the cationic and IL species. Then, the graphics shows important differences among those charges. Hence, Figure S2 (a) shows differences in the Mulliken charges on the S, O, C and F atoms belonging to anion and IL observing higher positive values on the S2, S3, C8 and C9 atoms and more negative values on the four O atoms of IL. Besides, the two S and C atoms present the same charges values in the IL but different in the anionic species while the Mulliken charges on the N1 atoms remains practically constant in the anion and IL and, only more negative charges values are observed on the six F atoms of IL. On the other side, Figure S2 (b) reveals differences in the MK charges on S2 and S3 atoms showing higher values for S3 in the anion and S2 in the IL. The charges on C8 atoms in both species are the same while the MK charge on C9 is higher in the IL. The MK charges on the four O atoms are more negative in the anion while the charges on O5 and O6 are less negative in the IL. The MK charges on the six F atoms are slightly higher in the anion than the observed in IL. On the contrary, Figure S2 (c) evidence practically the same NPA charges on all atoms of both species. Hence, the NPA charges have practically no influence on the properties of IL. These studies show that the different MK charges on two S and C atoms evidence different behaviours of [NTf$_2^-$] groups in the anion of IL and, hence, suggest different coordination modes of these groups in the IL while the same Mulliken charges values on those atoms suggest similar coordination modes of those groups in the IL.

When the molecular electrostatic potentials (MEPs) on N1 atom of the cation (-18.080 a.u.) is compared with the corresponding to IL (-18.196 a.u.) (see Table S1) a more negative value is observed in the IL. However, when the MEPs on the atoms of anion and IL are compared the values remain unchanged, as observed in **Figure S3**. This result is similar to what was observed forthe MK charge on N1 atom of cation , as expected because the MEP values are obtained from those MK charges [55]. Therefore, both MK charges and MEP values indicate that the incorporation of anion has influence on the cation in the formation of [Aliquat$^+$] [NTf$_2^-$] ionic liquid. If now the mapped MEP surfaces for the three species are compared in order to investigate the nucleophilic and electrophilic regions one can observe in Figure S4 that the mapped surface of cation is completely blue being stronger the coloration around the quaternary N, as expected because this species is positively charged. Hence, the cation is electrophilic while the mapped surface of anion is totally red due to that this species is negatively charged. Strong red colours are observed on the SO$_2$ groups of anion. Hence, the

anion is nucleophilic. On the contrary, the mapped surface of the IL shows less strong red and blue colorations on the SO_2 groups of anion and on the quaternary N of cation, respectively.

Another interesting property to investigate in the cation, anion and IL is the bond order (BO) expressed as Wiberg index. Thus, from Table S1 when the value for N1 atom of cation is compared with the corresponding value of IL we observed the same values (3.594); however, when the BOs of the atoms of anion are compared with the corresponding to IL the values slightly change for the S and O atoms while for the remain atoms the values are practically similar, as observed in **Figure S5**. These results show that possibly those S and O atoms belonging to [NTf$_2^-$] anion will be involved in the coordination modes to cation during the formation of IL and, for these reasons, the BOs values of those atoms change.

4.4. NBO and AIM studies

The presence of intra-molecular or H bonds interactions stabilize an ionic liquid, as observed in previous related studies [34,37,38] and, for these reasons, the second order perturbation theory analyses of Fock matrix in NBO Basis and the topological properties were calculated for the IL and its cationic and anionic species in gas phase by using the NBO and AIM 2000 programs, respectively [56-58]. Both calculations are important and useful to determine different transitions and ionic or H bond interactions. The interactions observed by NBO calculations for the cation present very low energies (<<<10 kcal/mol) and, for these reasons, they are no presented here. Therefore, calculated donor-acceptor energy interactions for anion and IL in gas phase at different levels of theory are observed in Table S2. Only, two types of interactions are observed in both species which are the $n{\rightarrow}\sigma^*$ and $\sigma^*{\rightarrow}\sigma^*$ interactions. In the former interactions transitions from lone pairs of N, O and F atoms corresponding to anion and IL to anti-bonding N-S, S-O, S-C and C-F orbitals are involved, as detailed in Table S2. Note that the energies of these interactions are higher in the IL (1856.42 kJ/mol), as compared with the observed for the anion (203.36 kJ/mol), while in the $\sigma^*{\rightarrow}\sigma^*$ interactions transitions from anti-bonding N-S and S-O orbitals to anti-bonding N-S and S-O orbitals are involved. These interactions are also higher in the IL than in the corresponding anion. Hence, the total energy clearly favours the IL (2317.22 kJ/mol) and reveals that cation increases in significant form the energy of the anion (366.84 kJ/mol) due to the additional transitions.

The topological properties allows to determine the nature of different interactions such as, intra-molecular, H bonds, ionic, covalent polar, etc., by using the AIM 2000 program and the Bader's theory of atoms in molecules [57,58]. The electron density, $\rho(r)$, the Laplacian

values, $\nabla^2\rho(r)$, the eigenvalues *(λ1, λ2, λ3)* of the Hessian matrix and, the $|λ1|/λ3$ ratio should be calculated in the bond critical points (BCPs) and ring critical points (RCPs). Thus, these calculations were performed for the cation, anion and IL in gas phase at different levels of theory. In the cationic species in gas phase no new interactions are observed, while for the anion and the IL in gas phase the topological properties are modified as reported in Table S3. In the anion, only an H bond interaction with characteristics corresponding to an ionic or highly polar covalent interaction can be seen where *λ1/λ3< 1* and $\nabla^2\rho(r) > 0$ (closed-shell interaction). The new S3-O6···F14 interaction formed in the anion is shown in the molecular graphic presented in **Figure S6** which form a RCP named RCPN. In the IL eleven new interactions are observed where only nine of them have characteristics of H bonds interactions and six of them are of type S-O···H, two of type C-H···H and one C-H···N, another is ionic, as observed in the cation (S2-O85···F90) and, another one is an halogen interaction (C11-H13···F93). Due to number of interactions and to the complexity of molecular graphic for the IL only some interactions can be observed in **Figure S7** but, all topological properties for those eleven interactions are presented in Table S3. Note that the closer distances between the involved atoms are observed in the two C-H···H interactions (2.159/2.151 Å) while the ionic interaction presents higher distance between the O and F atoms (3.170 Å). In the IL, three O atoms (O84, O86 and O87) of anionic species are coordinated to two H atoms by S-O···H interactions, as graphed in **Figure S8** by using the Moldraw program [65]. Hence, hexadentate coordination mode can be seen in the IL and, due to number of interactions present, this species is the more stable than the anionic one, as expected because the ionic charged species are unstable.

4.5. Frontier orbitals studies

Comparisons of calculated geometrical parameters for cation, anion and IL have shown that anion undergoes changes in the formation of IL, while the different MK charges observed on N1 atoms of cation and IL suggest that this property is modified in the IL. On the other hand, the interactions predicted in the IL by using NBO and AIM calculations reveal different characteristics and support a hexadentate coordination mode between cation and anion of IL. Hence, the high number of interactions and high dipole moment and volume values of IL justify its higher stability as compared to the cationic and anionic species. Now, in order to investigate the reactivities and behaviours of those three species in gas phase, the highest occupied molecular orbital (HOMO) and lowest unoccupied molecular orbital (LUMO) were calculated together with the energies of gap values and the chemical potential (μ),

electronegativity (χ), global hardness (η), global softness (S), global electrophilicity index (ω) and global nucleophilicity index (E) descriptors [34,37,38]. These results and the equations used to calculate the descriptors are presented in **Table S4**. The values for the three species are compared in **Table S5** with those reported for other ionic liquids such as, 1-ethyl-3-methylimidazolium hexafluorophosphate [34], 1-buthyl-3-methyl imidazolium nitrate [37] and 1-buthyl-3-methyl imidazolium trifluoromethanesulfonate [38]. Comparing first the gap values for cation and anion of [Aliquat$^+$][NTf$_2^-$] IL it is observed that cation gap (8.2152 eV) is higher than anion gap (7.2600 eV) and, that the anion produces a decrease in the gap value of IL (7.5158 eV). Therefore, the most reactive species with low gap value is the anion, in agreement with the low stabilization energy calculated by NBO analysis, while the less reactive species is the cation probably due to the three large side chains. The IL is more stable than the anion due to the eleven interactions observed by AIM analysis and to high number of transitions evidenced by NBO studies. If now the gap values for cation and anion of [Aliquat$^+$][NTf$_2^-$] IL are compared with [EMIM$^+$][PF$_6^-$] IL and its [EMIM$^+$] cation and [PF$_6^-$] anion [34], it is observed higher reactivities in [EMIM$^+$][PF$_6^-$] IL and its cation but the [PF$_6^-$] anion is less reactive than [NTf$_2^-$]. On the other side, both [BMIM][OTF] and [BMIM][NO$_3$] ILs are more reactive than the other ones being, 1-buthyl-3-methyl imidazolium nitrate the most reactive. Regarding the global electrophilicity index (ω) and global nucleophilicity index (E) the cation of [Aliquat$^+$][NTf$_2^-$] IL presents the higher values (ω = 4.7950 eV and E= -25.7805 eV), as compared with the anion and IL while the [EMIM$^+$] cation shows higher values (ω = 10.9934 eV and E= -28.6227 eV) than the other one.

4.6. Thermal analysis

The knowledge of the thermal properties of ILs is crucial from an engineering point of view as they are important parameters for determining process conditions. In order to obtain a comprehensive picture of the thermal behaviour, two complementary thermal analysis techniques were used. Firstly, knowing that [([Aliquat$^+$][NTf$_2^-$]) is liquids at room temperature, upon heating, we observed that the thermal decomposition occurs in the temperature range ≈ 360–500 °C, with a mass loss that reaches 83% at 483 °C.
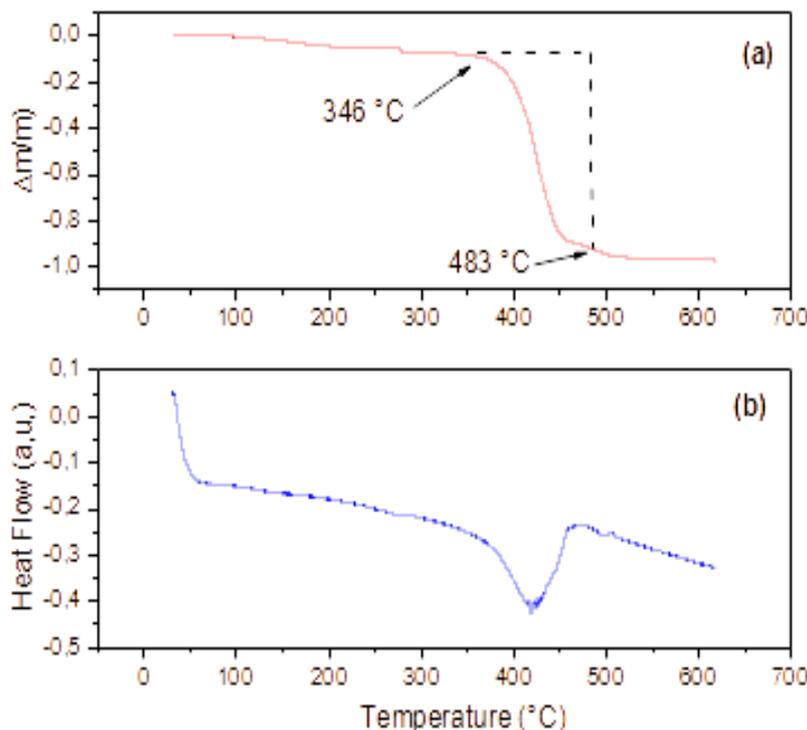
Figure 4. TGA (a) and DTA (b) curves of ([Aliquat$^+$][NTf$_2^-$]) ILs.

Comparing our TGA measurements of ([Aliquat$^+$][NTf$_2^-$]) with those reported by Mikkola et al [27], it can be noted that [([Aliquat$^+$][NTf$_2^-$]) is thermally more stable than [Aliquat$^+$] containing the nitrate [NO$_3^-$] (T_d = 202 °C), hexafluorophosphate [PF$_6^-$] (T_d = 274 °C) and tetrafluoroborate [BF$_4^-$] anion (T_d = 294 °C). Many previous studies indicated that the thermal stability of ionic liquids strongly depends on the type of anion [67], the fact that ([Aliquat$^+$] [NTf$_2^-$]) is thermally more stable than the cited ILs [27] can be explained by the high thermal stability of bis(trifluoromethylsulfonyl)imide anion, its larger size and molecular structure [31,66]. As reported in **Figure 4**, the DTA curves confirm that the decomposition temperature for ([Aliquat$^+$][NTf$_2^-$]) was found at 483 °C.

4.7. Vibrational studies

B3LYP/6-31G* calculations have optimized the cation and IL with C_1 symmetries while the anion was optimized with the same symmetry but by using the B3LYP/6-311++G** method. Due to the presence of 80 and 15 atoms in the structures of cation and anion, respectively, 234 and 39 vibration modes are expected in these species while in the IL a total of 279 vibration are expected . The vibration modes of the three species present activity in both infrared and Raman spectra. Here, the scaled quantum mechanical force field (SQMFF) methodology was

used to determine the force fields of cation and anion considering the corresponding normal internal coordinates, transferable scaling factors and the Molvib program [59-61] while the vibrational assignments for the ionic liquid were performed with the aid of *GaussView* program and, using a scale factor only for the vibration modes corresponding to the higher wavenumbers region [51]. In the definition of normal internal coordinates of cation the quaternary N atoms was considered with C_{3V} symmetry because that atoms is linked to three similar side chains and to a CH_3 groups. Vibrational measurements are carried out using FTIR-ATR and RAMAN techniques. In **Figures 5** and **6** we presented respectively the experimental ATR and Raman spectra of [Aliquat$^+$][NTf$_2^-$] IL in solid phase compared with the predicted for the cation, anion species and IL in gas phase by using the hybrid B3LYP method. A detailed investigation of the vibrational frequencies and the assignment of the observed bands are provided in **Table 3** and will be discussed in the following sub-sections.
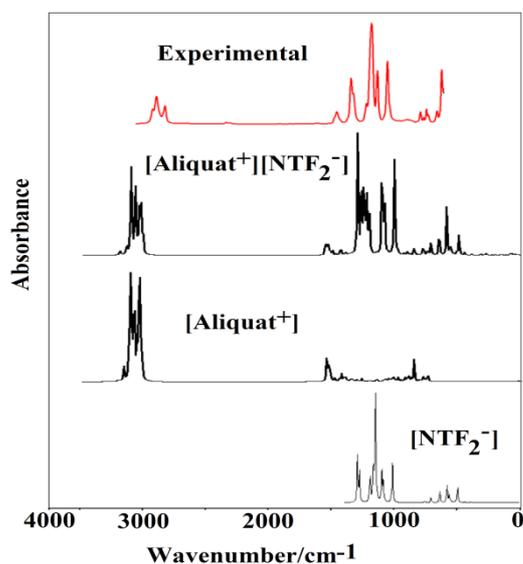
Figure 5. Experimental Infrared spectra of [Aliquat$^+$][NTf$_2^-$] IL in liquid phase compared with the predicted for the cation, anion and IL in gas phase by using the hybrid B3LYP method.
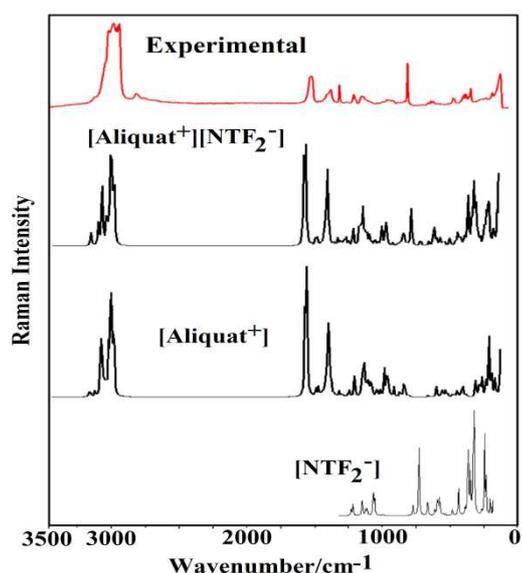
Figure 6. Experimental Raman spectra of [Aliquat$^+$][NTf$_2^-$] IL in liquid phase compared with the predicted for the cation, anion and IL in gas phase by using the hybrid B3LYP method.

Table 3. Observed and calculated wavenumbers (cm^{-1}) and assignments for [Aliquat$^+$][NTf$_2^-$] ionic liquid and its cation and anion in gas phase by using the hybrid B3LYP method and different basis sets.

Exp[a]		B3LYP method[a]					
		6-311++G**		6-31G*			
IR	Raman	[NTf$_2^-$]		[Aliquat$^+$]		[Aliquat$^+$][NTf$_2^-$]	
		SQM[b]	Assignments[a]	SQM[c]	Assignments[a]	SQM[d]	Assignments[a]

17

	3051vw	3081	ν_aCH$_3$(C77)	3088	ν_aCH$_3$
		3068	ν_aCH$_3$(C77)	3085	ν_aCH$_3$
		3032	ν_aCH$_2$(C30)	3081	ν_aCH$_2$
		3030	ν_aCH$_2$(C2)	3072	ν_aCH$_2$
		3023	ν_aCH$_2$(C5)	3040	ν_aCH$_2$
		2993	ν_aCH$_3$(C51)	3030	ν_aCH$_3$
2990sh		2992	ν_aCH$_3$(C26)	3021	ν_aCH$_3$
		2992	ν_aCH$_3$(C73)	3005	ν_aCH$_3$
		2987	ν_sCH$_2$(C2)	3003	ν_sCH$_2$
		2984	ν_sCH$_3$(C77)	3003	ν_sCH$_3$
		2982	ν_aCH$_3$(C51)	3002	ν_aCH$_3$
		2982	ν_aCH$_3$(C26)	3000	ν_aCH$_3$
	2980sh	2980	ν_aCH$_3$(C73)	2998	ν_aCH$_3$
		2980	ν_sCH$_2$(C30)	2997	ν_sCH$_2$
	2977sh	2976	ν_aCH$_2$(C55)	2997	ν_aCH$_2$
		2975	ν_aCH$_2$(C8)	2997	ν_aCH$_2$
2971w		2973	ν_aCH$_2$(C33)	2993	ν_aCH$_2$
	2967sh	2967	ν_sCH$_2$(C5)	2991	ν_sCH$_2$
2956sh		2962	ν_aCH$_2$(C36)	2976	ν_aCH$_2$
	2953vs	2953	ν_aCH$_2$(C58)	2968	ν_aCH$_2$
		2953	ν_aCH$_2$(C17)	2967	ν_aCH$_2$
		2952	ν_aCH$_2$(C64)	2966	ν_aCH$_2$
2944w		2949	ν_aCH$_2$(C42)	2965	ν_aCH$_2$
		2942	ν_aCH$_2$(C11)	2964	ν_aCH$_2$
		2936	ν_aCH$_2$(C70)	2963	ν_aCH$_2$
		2935	ν_aCH$_2$(C48)	2961	ν_aCH$_2$
		2933	ν_sCH$_2$(C55)	2951	ν_sCH$_2$
		2932	ν_sCH$_2$(C8)	2950	ν_sCH$_2$
		2932	ν_sCH$_2$(C33)	2949	ν_sCH$_2$
		2931	ν_aCH$_2$(C23)	2946	ν_aCH$_2$
		2930	ν_aCH$_2$(C61)	2945	ν_aCH$_2$
2922sh	2918vs	2920	ν_aCH$_2$(C14)	2939	ν_aCH$_2$
		2920	ν_sCH$_3$(C26)	2937	ν_sCH$_3$
		2920	ν_sCH$_3$(C51)	2936	ν_sCH$_3$
		2919	ν_sCH$_2$(C36)	2936	ν_sCH$_2$
		2919	ν_sCH$_3$(C73)	2935	ν_sCH$_3$
		2916	ν_aCH$_2$(C67)	2933	ν_aCH$_2$
		2914	ν_aCH$_2$(C45)	2932	ν_aCH$_2$
		2913	ν_aCH$_2$(C20)	2931	ν_aCH$_2$
		2910	ν_aCH$_2$(C39)	2929	ν_aCH$_2$
		2909	ν_sCH$_2$(C11)	2927	ν_sCH$_2$
		2909	ν_sCH$_2$(C58)	2925	ν_sCH$_2$
		2908	ν_sCH$_2$(C70)	2924	ν_sCH$_2$
		2907	ν_sCH$_2$(C48)	2922	ν_sCH$_2$
		2904	ν_sCH$_2$(C23)	2918	ν_sCH$_2$
		2901	ν_sCH$_2$(C64)	2918	ν_sCH$_2$
		2900	ν_sCH$_2$(C42)	2916	ν_sCH$_2$
	2873vs	2898	ν_sCH$_2$(C61)	2915	ν_sCH$_2$
		2898	ν_sCH$_2$(C14)	2909	ν_sCH$_2$

18

		2893	$\nu_sCH_2(C17)$	2909	ν_sCH_2
2890sh		2890	$\nu_sCH_2(C67)$	2907	ν_sCH_2
		2890	$\nu_sCH_2(C45)$	2907	ν_sCH_2
		2890	$\nu_sCH_2(C20)$	2906	ν_sCH_2
2874w	2747w	2886	$\nu_sCH_2(C39)$	2903	ν_sCH_2
		1496	$\delta CH_2(C42)$ $\delta C39C42C45$	1558	$\delta CH2,\delta C39C42C45$
1491sh	1487sh	1486	$\delta_aCH_3(C77)$	1546	δ_aCH_3
	1476sh	1476	$\delta CH_2(C17)$ $\delta CH_2(C14)$	1545	δCH_2
		1475	$\delta CH_2(C55)\delta CH_2(C58)$	1544	δCH_2
		1474	$\delta_aCH_3(C73)$	1542	δ_aCH_3
		1473	$\delta_aCH_3(C26)$	1541	δ_aCH_3
1472w		1472	$\delta_aCH_3(C51)$	1539	δ_aCH_3
	1466sh	1465	$\delta_aCH_3(C51)$	1538	δ_aCH_3
		1465	$\delta_aCH_3(C73)$	1534	δ_aCH_3
		1465	$\delta CH_2(C30)$ $\delta CH_2(C2)$	1532	δCH_2
		1464	$\delta CH_2(C8)$	1531	δCH_2
		1464	$\delta_aCH_3(C26)$	1531	δ_aCH_3
		1462	$\delta CH_2(C36)$ $\delta CH_2(C39)$	1531	δCH_2
		1462	$\delta CH_2(C64)$	1531	δCH_2
		1461	$\delta_aCH_3(C77)$	1530	δ_aCH_3
		1459	$\delta CH_2(C39)$ $\delta CH_2(C58)$	1530	δCH_2
		1457	$\delta CH_2(C33)$	1528	δCH_2
		1457	$\delta CH_2(C45)$	1526	δCH_2
		1454	$\delta CH_2(C2)$	1523	δCH_2
1452sh	1452m	1453	$\delta CH_2(C55)$ $\delta CH_2(C8)$	1520	δCH_2
		1450	$\delta CH_2(C70)$ $\delta CH_2(C48)$	1518	δCH_2
		1450	$\delta CH_2(C48)$	1518	δCH_2
		1450	$\delta CH_2(C70)$ $\delta CH_2(C23)$	1517	δCH_2
		1447	$\delta CH_2(C17)\delta CH_2(C14)$	1517	δCH_2
		1447	$\delta CH_2(C67)$	1516	δCH_2
		1446	$\delta CH_2(C36)$ $\delta CH_2(C39)$	1515	$\delta CH_2,$
		1446	$\delta CH_2(C61)$	1514	δCH_2
		1446	$\delta CH_2(C20)$ $\delta CH_2(C11)$	1514	δCH_2
		1441	$\delta CH_2(C5)\delta CH_2(C30)$	1513	δCH_2
	1434sh	1432	$wagCH_2(C30)$	1511	$wagCH_2$
	1423sh	1423	$\rho CH_2(C2)$	1498	ρCH_2
		1407	$wagCH_2(C45)$	1473	$wagCH_2$
		1406	$wagCH_2(C67)$	1443	$wagCH_2$
		1404	$wagCH_2(C39)$ $wagCH_2(C42)$	1442	$wagCH_2$
		1402	$wagCH_2(C58)$ $wagCH_2(C61)$	1442	$wagCH_2$
		1401	$wagCH_2(C20)$ $wagCH_2(C11)$	1439	$wagCH_2$
		1395	$wagCH_2(C14)$	1436	$wagCH_2$
		1394	$\delta_sCH_3(C77)$	1434	δ_sCH_3
		1388	$wagCH_2(C5)$	1429	$wagCH_2$
		1385	$\delta_sCH_3(C73)$	1427	δ_sCH_3
		1383	$\delta_sCH_3(C51)$	1427	δ_sCH_3
		1381	$\delta_sCH_3(C26)$	1426	δ_sCH_3
		1372	$wagCH_2(C36)$	1421	$wagCH_2$
		1371	$wagCH_2(C64)$ $wagCH_2(C70)$	1403	$wagCH_2$

				1365	wagCH$_2$(C14)wagCH$_2$(C5)	1398	wagCH$_2$
				1362	wagCH$_2$(C55)	1395	wagCH$_2$
1357m	1354sh			1359	ρCH$_2$(C5) ρCH$_2$(C30)	1386	ρCH$_2$
				1344	wagCH$_2$(C33) ρCH$_2$(C36)	1375	wagCH$_2$, ρCH$_2$
1339sh				1336	wagCH$_2$(C23)	1373	wagCH$_2$
	1329sh			1329	wagCH$_2$(C2) ρCH$_2$(C55)	1368	wagCH$_2$, ρCH$_2$
				1328	wagCH$_2$(C48)	1363	wagCH$_2$
				1324	ρCH$_2$(C58) ρCH$_2$(C61)	1360	ρCH$_2$
1318sh				1316	ρCH$_2$(C39) ρCH$_2$(C48)	1358	ρCH$_2$
				1316	ρCH$_2$(C67)	1357	ρCH$_2$
				1315	ρCH$_2$(C11)	1353	ρCH$_2$
				1314	ρCH$_2$(C45) ρCH$_2$(C42)	1351	ρCH$_2$
1309sh				1310	ρCH$_2$(C23)ρCH$_2$(C8)	1349	ρCH$_2$
	1305w			1307	ρCH$_2$(C70)ρCH$_2$(C64)	1346	ρCH$_2$
				1304	ρCH$_2$(C23) ρCH$_2$(C30)	1346	ρCH$_2$
				1297	wagCH$_2$(C67)wagCH$_2$(C55)	1343	wagCH$_2$
	1293sh			1292	ρCH$_2$(C48) ρCH$_2$(C36)	1337	ρCH$_2$
				1285	wagCH$_2$(C8)	1332	wagCH$_2$
				1280	ρCH$_2$(C14)	1328	ρCH$_2$
				1272	ρCH$_2$(C70)	1313	ρCH$_2$
				1265	ρCH$_2$(C30)	1309	ρCH$_2$
	1253sh			1263	wagCH$_2$(C58)	1303	wagCH$_2$
				1247	ρCH$_2$(C36) wagCH$_2$(C42)	1302	ρCH$_2$, wagCH$_2$
	1242m	1236	ν$_a$SO$_2$(S2)	1237	ρCH$_2$(C20)	1299	ν$_a$SO$_2$(S2)
1230sh	1232sh			1230	wagCH$_2$(C14)	1292	wagCH$_2$
				1226	ρCH$_2$(C33)	1285	ρCH$_2$
1187vs	1187vw	1221	ν$_a$SO$_2$(S3)	1220	ρCH$_2$(C64) ρCH$_2$(C67)	1271	ν$_a$SO$_2$(S3)
				1188	ρ'CH$_3$(C77)	1269	ρ'CH$_3$
1177sh				1181	ρCH$_2$(C14)	1267	ρCH$_2$
1168sh				1168	ρCH$_2$(C39)	1258	ρCH$_2$
1140s		1157	ν$_s$CF$_3$(C9)	1164	ρCH$_3$(C77)	1254	ν$_s$CF$_3$
	1134w	1150	ν$_s$CF$_3$(C8)	1143	ρ'CH$_3$(C77)	1250	ν$_s$CF$_3$
1130sh		1124	ν$_a$CF$_3$(C9)	1128	ρCH$_3$(C51)	1241	ν$_a$CF$_3$
1126sh	1122sh	1120	ν$_a$CF$_3$(C8)	1126	ρCH$_3$(C51)	1228	ν$_a$CF$_3$
	1108sh	1108	ν$_a$CF$_3$(C9)	1109	ρCH$_3$(C73)	1217	ν$_a$CF$_3$
		1104	ν$_a$CF$_3$(C8)	1101	ρCH$_3$(C73)	1206	ν$_a$CF$_3$
	1094sh			1096	τwCH$_2$(C36)	1159	τwCH$_2$
1076sh	1077w			1083	ρ'CH$_3$(C26)	1149	ρ'CH$_3$
				1063	νC2-C55	1108	νC2-C55
1058s	1058sh	1056	νs$_a$SO$_2$(S2)	1059	νC5-C8	1104	νs$_a$SO$_2$
1049sh				1050	νC61-C64νC64-C67	1092	νC-C
1044sh	1042sh	1041	νs$_a$SO$_2$(S3)	1042	νC36-C39νC39-C42	1086	νs$_a$SO$_2$
				1039	νC45-C48νC42-C45νC48-C51	1082	νC-C
1037sh				1037	νC58-C61	1078	νC-C
				1034	νC17-C20	1076	νC-C
1030sh				1029	δC33C36C39	1075	δC33C36C39
				1026	νC11-C14νC14-C17	1072	νC-C
				1025	νC67-C70	1071	νC-C
				1013	νC30-C33	1060	νC-C

20

				1013	νC70-C73	1056	νC-C
				1008	νC55-C58	1052	νC-C
				1005	νC8-C11νC23-C26	1048	νC-C
	1000sh			1000	νC55-C58	1029	νC-C
				988	νC5-C8	1022	νC-C
				981	νC58-C61	1016	νC-C
				977	νaNC3	1010	νaNC3
		970	νS2-N1	970	νC17-C20	1006	νaS-N
	962vw			958	νN1-C77	1002	νN-C
				933	νC61-C64	987	νC-C
	924sh			926	νaNC3	982	νaNC3
				920	νC33-C36 ρ'CH3(C51)	977	νC-C, ρ'CH3
895vw				893	ρCH3(C73) νC67-C70	935	ρCH3, νC-C
	887w			885	ρCH3(C51)	928	ρCH3
				881	ρCH3(C26) νC20-C23	906	ρCH3, νC-C
874vw	870w			872	ρCH3(C51)	898	ρCH3
				865	ρ'CH3(C73)	891	ρ'CH3
				858	τwCH2(C20)	880	τwCH2
	845w			844	νaNC3	849	νaNC3
				835	τwCH2(C20) τwCH2(C14)	818	τwCH2
				825	τwCH2(C36)	809	τwCH2
790w	811			801	νaNC3	798	νaNC3
765vw	760vw			758	νsNC3	783	νsNC3
741w	737s	732	δsCF3(C9)	732	τwCH2(C64)	778	δsCF3
730sh				730	τwCH2(C30)τwCH2(C36)	769	τwCH2
716sh	725sh	723	δsCF3(C8)	725	τwCH2(C5)	760	δsCF3
				706	τwCH2(C2) τwCH2(C61)	746	τwCH2
				702	τwCH2(C33)τwCH2(C30)	744	τwCH2
		684	νS3-N1	686	τwCH2(C23) τwCH2(C20)	743	τwCH2
				675	τwCH2(C58)τwCH2(C55)	739	τwCH2
				671	τwCH2(C48)	735	τwCH2
				669	τwCH2(C11) τwCH2(C8)	714	νsS-N
		616	wagSO2(S3)	663	τwCH2(C67) τwCH2(C70)	648	wagSO2
655w		568	wagSO2(S2)	660	τwCH2(C42)τwCH2(C39)	587	wagSO2
618s	584vw	550	δaCF3(C9)	585	δC8C5N1 δN1C30C33	560	δaCF3
	565vw	540	δaCF3(C9)	533	δN1C2C55 δC58C61C64	554	δaCF3
	547vw	538	δaCF3(C8)	509	δaNC3	548	δaCF3
	507vw	528	δaCF3(C8)	499	δC36C39C42	534	δaCF3
		497	δSO2(S3)	475	δC36C39C42	508	δSO2
		483	δSO2(S2)	460	δsNC3	490	δSO2
	436vw			433	δC33C36C39 δC45C48C51	487	δCCC
				428	δC2C55C58	475	δCCC
	413sh			416	τC11-C14	444	τC-C
	399w	409	τwSO2(S3)	396	δC67C70C73δC61C64C67	440	τwSO2
	378sh			373	δC30C33C36	400	δCCC
		366	τwSO2(S2)	360	δC42C45C48	388	τwSO2
		331	ρSO2(S3)	359	ρ'NC3	337	ρSO2
	342sh	310	ρCF3(C9)	341	δaNC3 δaNC3	319	ρCF3
	328sh	303	ρCF3(C8)	335	δaNC3	315	ρCF3

21

304w	284	ρSO$_2$(S2)	278	δC11C14C17δC20C23C26	289	ρSO$_2$
227m	259	νS3-C9	269	δC55C58C61	274	νS-C
258sh	252	νS2-C8	248	δC36C39C42τC30-C33	263	ρCF$_3$
			240	τ$_w$CH$_3$(C77)	255	τ$_w$CH$_3$
			228	τC61-C64	254	τ$_w$CH$_3$
			225	τ$_w$CH$_3$(C51) δC33C36C39	250	τ$_w$CH$_3$
			223	τ$_w$CH$_3$(C26)	247	τC-C
			223	τ$_w$CH$_3$(C51)	230	τC-C
			213	τ$_w$CH$_3$(C73)	203	τC-C
203sh			197	τC14-C17	201	τC-C
	187	ρ'CF$_3$(C9)	195	τC58-C61δC64C67C70	198	ρ'CF$_3$
	186	ρ'CF$_3$(C8)	183	δC17C20C23	195	τ$_w$CH$_3$
173sh	163	δN1S3C9	172	τC33-C36	168	δSNS
156sh	149	δN1S2C8	158	τC5-C8	146	τC-C
			137	τC39-C42	141	τC-C
			132	τC45-C48	134	τC-C
121sh			118	τC42-C45	122	τC-C
			112	τC67-C70	116	τC-C
109w			109	τC8-C11	113	τC-C
	100	δS2N1S3	105	τC2-C55τC30-C33	105	τSNO
			99	τC5-C8τC30-C33	96	τC-C
			95	τC5-C8τC2-C55	84	τC-C
87sh			88	τC5-C8τC8-C11	76	τC-C
76sh			78	τC11-C14τC5-C8	73	τC-C
			74	τC20-C23	69	τC-C
63sh	60	τS2-N1	62	τC30-C33	66	τC-C
			55	τC64-C67	63	τC-C
49s			48	τC58-C61τ$_w$NC$_3$	53	τC-C, τ$_w$NC$_3$
			45	τC36-C39	47	τC36-C39
34sh	38	τ$_w$CF$_3$(C9)	40	τC17-C20	45	τ$_w$CF$_3$
	30	τ$_w$CF$_3$(C8)	30	τC58-C61τC5-C8	42	τ$_w$CF$_3$
15sh	5	τS3-N1	18	τ$_w$NC$_3$τC2-C55	7	τS-N

Abbreviations: ν, stretching; wag, wagging; τ, torsion; ρ, rocking; τ$_w$, twisting; δ, deformation; a, antisymmetric; s, symmetric; [a]This work, [b]From scaled quantum mechanical force field with B3LYP/6-311++G** method, [c]From scaled quantum mechanical force field with B3LYP/6-31G* method; [d]From B3LYP/6-31G* method.

4.7.1. Bands assignments

4.7.1.1. 4000-2000 cm^{-1} region. In this region, no bands of the anion are expected and only vibartional bands for the cation and the IL are predicted. The anti-symmetric and symmetric stretching modes of CH$_2$ and CH$_3$ groups are expected in this region. In the [Aliquat$^+$][Cl$^-$] IL the terminal CH$_3$ experimental anti-symmetric stretching band was observed at 2954 cm^{-1} and in [Aliquat$^+$][NTf$_2^-$] at 2956 cm^{-1}, respectively [68,69]. Here, this IL has four terminal CH$_3$ groups (C26, C51, C73, C77) where three of them belong to larges side chains (C26, C51, C73) and the remains belong to N-CH$_3$ group (C77). The SQMFF calculations predict the two anti-symmetric modes of latter group at higher wavenumbers than the other ones and, for

these reasons, the very weak Raman band at 3051 cm^{-1} is assigned to those vibration modes. The anti-symmetric stretching modes for the other CH$_3$ groups are predicted mixed with the anti-symmetric modes of CH$_2$ groups. The detailed assignments of these groups taking into account the SQM calculations can be seen in Table 3.

4.7.1.2. 1500-1000 cm^{-1} region. In this region the vibration modes of anion, cation and IL appear. Thus, the anti-symmetric SO$_2$ stretching modes of both groups are predicted at 1236 and 1221 cm^{-1} and, hence, the Raman and IR bands respectively at 1242 and 1187 cm^{-1} are assigned to those two vibration modes. The corresponding symmetric modes are predicted at 1056 and 1041 cm^{-1} and assigned respectively to the band and shoulder located at 1058 and 1044 cm^{-1}. In the IL, the anti-symmetric modes are predicted at 1299 and 1271 cm^{-1} while the symmetric ones at 1104 and 1086 cm^{-1}. The six anti-symmetric and symmetric stretching modes of two CF$_3$ groups are predicted by SQM calculations between 1157 and 1104 cm^{-1} while in the IL these modes are predicted between 1254 and 1206 cm^{-1}. Hence, the IR and Raman bands observed in that region are easily assigned to those stretching modes. In this region, for the cation the deformation, wagging and rocking modes of CH$_2$ groups and, the anti-symmetric and symmetric deformation and rocking modes of CH$_3$ groups are expected. The deformation modes of both groups appear mixed among them in the region between 1496 and 1381 cm^{-1}, thus, the bands and shoulders observed in that region can be assigned to those deformation modes. The wagging modes of CH$_2$ groups are predicted from 1432 up to 1230 cm^{-1} while the rocking modes between 1423 and 1168 cm^{-1} and, hence, those two vibration modes can be assigned, as predicted the SQM calculations and according assignments for similar species [34,37,38]. The rocking modes of CH$_3$ groups in the cation are predicted in this region between 1188 and 1083 cm^{-1} while in the IL between 1269 and 1149 cm^{-1}. Other rocking modes in the cation are also predicted between 920 and 865 cm^{-1} and in the IL between 977 and 891 cm^{-1}. Therefore, the IR and Raman bands and shoulders located in those regions are assigned to those rocking modes. Note that in this region are also predicted C-C stretching modes and CCC deformation modes.

4.7.1.3. 1000-10 cm^{-1} region. In this region the C-C and N-C stretching modes of cation and IL and the S-N stretching modes of anion are expected. Besides, the deformation, rocking and twisting modes of SO$_2$ groups and deformation modes of CF$_3$ groups of anion are predicted in this region together with the twisting modes of CH$_2$ and CH$_3$ groups of cation. The N-CH$_3$ stretching mode is predicted in the anion at 958 cm^{-1} and at 1002 cm^{-1} in the IL. Hence, the weak Raman band at 962 cm^{-1} is assigned to that vibration mode of both species. The S-N stretching mode is predicted in the anion at 684 cm^{-1} while in IL at 714 cm^{-1}.Hence, the IR and

Raman bands at 655 and 737 cm^{-1} respectively can be assigned to the symmetric deformation of CF$_3$ group and to the wagging mode of SO$_2$ group of anion and IL, respectively [70]. Both bands can also be simultaneously assigned to CH$_2$ twisting modes of cation. As reported in literature, the medium band around 790 cm^{-1} can be assigned to vibrations related to the N-C group [71].The strong band at 618 cm^{-1} is attributed to anti-symmetric deformation of CF$_3$ group of anion and IL. The deformation, rocking and twisting modes of SO$_2$ groups are assigned as predicted by calculations at 497/483, 331/284 and 409/366 cm^{-1} while the deformation and rocking modes of CF$_3$ groups can be assigned to the bands located between 550/528 and 310/303 cm^{-1}, respectively.

4.8. Force Fields

The harmonic force fields calculated with the SQMFF methodology and the Molvib program, for the anion of IL with the B3LYP/6-311++G** method and for its cation with the B3LYP/6-31G* level of theory, have allowed the determination of scaled force constants for those two species of IL in gas phase. These parameters are important to characterize the force of different bonds.In Table 4 the results of main force constants are compared with those reported for the [BMIM][OTF] IL and its cationic and anionic species [38].

Table 4. Scaled internal force constants for cation and anion of [Aliquat$^+$][NTf$_2$$^-$] in gas phase by using the B3LYP method and different basis sets.

Force constants	B3LYP Method 6-311++G**		
	[NTf$_2$$^-$] [a]	[OTF] [b]	[BMIM][OTF] [b]
f(νSO$_2$)	8.20	7.63	7.65
f(νCF$_3$)	5.31	4.98	5.20
f(νS-C)	2.16	2.03	2.21
f(νS-N)	4.56		
f(δSO$_2$)	1.93	1.62	1.82
f(δCF$_3$)	1.51	1.54	1.23
f(δS-N-S)	0.79		
Force constants	6-31G*	6-311++G**	
	[Aliquat$^+$] [a]	[BMIM] [b]	[BMIM][OTF] [b]
f(νN-CH$_3$)	3.95	4.40	5.06
f(νCH$_2$)	4.75	4.73	4.73
f(νCH$_3$)	4.91	4.87	4.84
f(δCH$_2$)	0.79	0.77	1.28
f(δCH$_3$)	0.56	0.52	0.54

Units are mdyn Å^{-1} for stretching and mdyn Å rad^{-2} for angle deformations.

[a]This work, [b]From Ref [38] for [BMIM][OTF].

Analyzing first the force constants of anionic species of both ILs, we observed higher values in the f(νSO$_2$) and f(νCF$_3$) force constants, as expected because the [NTf$_2$$^-$] anion presents two

SO$_2$ and two CF$_3$ groups while [OTF] has only one SO$_3$ and one CF$_3$ group [38]. However, the values of those two force constants increase in the [BMIM][OTF] IL. Comparing now the cationic species of both ILs, it is observed that despite of three long side chains present in [Aliquat$^+$] the values of all force constants are practically the same and only a slight lower value is observed in the *f(vN-CH$_3$)* force constant. This minimum difference could be explained in [Aliquat$^+$] because the N atom of group is not linked to a ring, as in [BMIM] [38]. In the [BMIM][NO$_3$] IL, the value of the *f(vN-CH$_3$)* force constant is 4.70 mdyn Å^{-1} [37] while in the free base of alkaloids as scopolamine, the value is 4.76 mdyn Å^{-1} and, in heroin and morphine the value increase at 4.83 mdyn Å^{-1} [72-74]. In all those alkaloids, the N atom of N-CH$_3$ group is part of a ring.

5. Conclusions

[Aliquat$^+$][NTf$_2$$^-$] IL is successfully synthesized by anionic exchange of [Aliquat$^+$][Cl$^-$]. Its structure was confirmed by [1]H-NMR, [13]C-NMR, and [19]F-NMR spectroscopy and characterized it by infrared and Raman spectroscopies. The thermal stability of this IL was investigated by TGA and DTA measurements. The thermal behaviour indicated that [Aliquat$^+$][NTf$_2$$^-$] is stable up to 483°C. The structures of cation and IL were determined by theoretical B3LYP/6-31G* calculations while the anionic species was optimized by using the B3LYP/6-311++G** level of theory. A hexadentate coordination geometry between cation-anion was predicted by atoms in molecules (AIM) studies for the [Aliquat$^+$][NTf$_2$$^-$] IL by using B3LYP/6-31G* calculations where three O atoms of anion are linked to six H atoms of cation by S-O···H interactions. Changes in the bond orders of S and O atoms of cation of IL support such observations. The predict cation-anion distances are in the range 2.30-2.60 Å. The MK charge on N atom of cation (0.133 a.u.) is different from that observed on the IL (-0.376 a.u.) in accordance to the corresponding MEP values. The frontier orbital studies predict that gap cation (8.2152 eV) is higher than gap anion (7.2600 eV) and, hence, the anion is the most reactive species, in agreement with the low stabilization energy calculated by NBO analysis, while the less reactive species is the cation probably due to the three long side chains. The harmonic force fields of cation and anion were calculated by using the SQMFF methodology and the complete assignments of 234 and 39 vibration modes expected for the cation and anion respectively were performed. The scaled force constants of both species were also reported. Then, the most important bands observed in the infrared and Raman spectra of IL were assigned.

Supplementary Information (SI)

Supplementary Information: **Table S1-S5 and Figures S1-S8.**

REFERENCES

[1] S.F. Ghasemi Gildeh, H. Roohi, M. Mehrdad, K. Rad-Moghadam, K. Ghauri, Experimental and theoretical probing of the physicochemical properties of ionic liquids composed of [Bn-DBU]+ cation and various anions, *Journal of Molecular Structure* 1202 (2020) 127226.

[2] M. Ahrenberg, M. Beck, C. Neise, O. Keßler, U. Kragl, S.P. Verevkin, C. Schick, Vapor pressure of ionic liquids at low temperatures from AC-chip-calorimetry, *Physical Chemistry Chemical Physics* 18(31) (2016) 21381-21390.

[3] L. Ni, J. Xin, K. Jiang, L. Chen, D. Yan, X. Lu, S. Zhang, One-Step Conversion of Biomass-Derived Furanics into Aromatics by Brønsted Acid Ionic Liquids at Room Temperature, *ACS Sustainable Chemistry & Engineering* 6(2) (2018) 2541-2551.

[4] M. Bystrzanowska, F. Pena-Pereira, Ł. Marcinkowski, M. Tobiszewski, How green are ionic liquids? – A multicriteria decision analysis approach, *Ecotoxicology and Environmental Safety* 174 (2019) 455-458.

[5] B.-S. Lee, S.-T. Lin, Prediction and screening of solubility of pharmaceuticals in single- and mixed-ionic liquids using COSMO-SAC model, *AIChE Journal* 63(7) (2017) 3096-3104.

[6] Y. Zhou, D. Xu, L. Zhang, Y. Ma, X. Ma, J. Gao, Y. Wang, Separation of thioglycolic acid from its aqueous solution by ionic liquids: Ionic liquids selection by the COSMO-SAC model and liquid-liquid phase equilibrium, *The Journal of Chemical Thermodynamics* 118 (2018) 263-273.

[7] R.L. Vekariya, A review of ionic liquids: Applications towards catalytic organic transformations, *Journal of Molecular Liquids* 227 (2017) 44-60.

[8] J.Nawała, , B.Dawidziuk, , D.Dziedzic, , D.Gordon, , & S. Popiel, Applications of ionic liquids in analytical chemistry with a particular emphasis on their use in solid-phase microextraction. *TrAC Trends in Analytical Chemistry 105* (2018) 18-36.

[9] M. Watanabe, M.L. Thomas, S. Zhang, K. Ueno, T. Yasuda, K. Dokko, Application of Ionic Liquids to Energy Storage and Conversion Materials and Devices, *Chemical Reviews* 117(10) (2017) 7190-7239.

[10] Y. Qiang, S. Zhang, L. Guo, X. Zheng, B. Xiang, S. Chen, Experimental and theoretical studies of four allyl imidazolium-based ionic liquids as green inhibitors for copper corrosion in sulfuric acid, *Corrosion Science* 119 (2017) 68-78.

[11] G. K.Dedzo, B. B.Nguelo, I. T.Kenfack, E.Ngameni, , C. Detellier, Molecular control of the functional and spatial interlayer environment of kaolinite by the grafting of selected pyridinium ionic liquids. *Applied Clay Science* (2017) *143* 445-451.

[12] Q. Zhou, F. Chen, W. Wu, R. Bu, W. Li, F. Yang, Reactive orange 5 removal from aqueous solution using hydroxyl ammonium ionic liquids/layered double hydroxides intercalation composites, *Chemical Engineering Journal* 285 (2016) 198-206.

[13] Y. Pei, Q. Lu, Y. Niu, Y. Zhao, Y. Zhao, Z. Li, H. Wang, J. Wang, Aggregation Behavior of Pyrrolidinium Ionic Liquid Surfactants in −OH-Functionalized Ammonium-Based Protic Ionic Liquids, *Journal of Chemical & Engineering Data* 64(11) (2019) 4708-4716.

[14] C. Verma, E.E. Ebenso, M.A. Quraishi, Ionic liquids as green and sustainable corrosion inhibitors for metals and alloys: An overview, *Journal of Molecular Liquids* 233 (2017) 403-414.

[15] J. Cai, J. Liu, S. Mu, J. Liu, J. Hong, X. Zhou, Q. Ma, L. Shi, Corrosion Inhibition Effect of Three Imidazolium Ionic Liquids On Carbon Steel In Chloride Contaminated Environment, *Int. J. Electrochem. Sci* 15 (2020) 1287-1301.

[16] Fraile, J. M., García, J. I., Herrerías, C. I., Mayoral, J. A., Carrié, D., & Vaultier, M. (2001). Enantioselective cyclopropanation reactions in ionic liquids. *Tetrahedron: Asymmetry*, *12*(13), 1891-1894.

[17] X.-S. Lin, Y. Zou, K.-H. Zhao, T.-X. Yang, P. Halling, Z. Yang, Tetraalkylammonium ionic liquids as dual solvents–catalysts for direct synthesis of sugar fatty acid esters, *Journal of Surfactants and Detergents* 19(3) (2016) 511-517.

[18] C. A.Migdal, , P. E.Stott, , V. N.Bakunin, , O. P.Parenago, , G. N. Kuz'mina, , L. M.Vedeneeva, , & A. Y. Suslov, *U.S. Patent No. 6,878,676.* (2005) Washington, DC: U.S. Patent and Trademark Office.

[19] A. Rout, K. Binnemans, Separation of rare earths from transition metals by liquid–liquid extraction from a molten salt hydrate to an ionic liquid phase, *Dalton Transactions* 43(8) (2014) 3186-3195.

[20] M. Filiz, N.A. Sayar, A.A. Sayar, Extraction of cobalt (II) from aqueous hydrochloric acid solutions into alamine 336–m-xylene mixtures, *Hydrometallurgy* 81(3-4) (2006) 167-173.

[21] R. Banda, H.Y. Lee, M.S. Lee, Separation of Zr from Hf in hydrochloric acid solution using amine-based extractants, *Industrial & engineering chemistry research* 51(28) (2012) 9652-9660.

[22] G. Naz, Z. Othaman, M. Shamsuddin, S.K. Ghoshal, Gold nanorod libraries enhancement for optical imaging, *Materials Letters* 166 (2016) 63-66.

[23] A. Patra, T. Mahapatra, Synthesis of tetrahydrobenzo [b] pyran derivatives catalysed by Aliquat® 336 in water under microwave irradiation, *Journal of Chemical Research* 34(12) (2010) 689-693.

[24] M. Mateescu, I.C. Bujanca, M. Deaconu, The application of aliquat 336 as carrier in processes for wastewater treatment containing heavy metals 2017 (2017) 125-125.

[25] Assenine, M. A., Haddad, B., Paolone, A., Brandán, S. A., Villemin, D., Boumediene, M., ... & Bresson, S. (2020). Experimental and DFT studies on structure, spectroscopic and thermal properties of N-Methyl-N, N, N-trioctylammonium chloride ionic liquid. Journal of Molecular Structure, 129625.

[26] Blanco, D., Oulego, P., Ramos, D., Fernández, B., & Cuetos, J. M. (2017). Model-free kinetics applied to evaluate the long-term thermal stability of three [NTf2] anion-based ionic liquids. *Thermochimica Acta*, *656*, 70-84.

[27] J.-P. Mikkola, P. Virtanen, R. Sjöholm, Aliquat 336®—a versatile and affordable cation source for an entirely new family of hydrophobic ionic liquids, *Green Chemistry* 8(3) (2006) 250-255.

[28] B.Haddad, D. Mokhtar, M. Goussem, E.-h. Belarbi, D. Villemin, S. Bresson, M. Rahmouni, N.R. Dhumal, H.J. Kim, J. Kiefer, Influence of methyl and propyl groups on the vibrational spectra of two imidazolium ionic liquids and their non-ionic precursors, *Journal of Molecular Structure* 1134 (2017) 582-590.

[29] B. Haddad, J. Kiefer, H. Brahim, E.-h. Belarbi, D. Villemin, S. Bresson, O. Abbas, M. Rahmouni, A. Paolone, O. Palumbo, Effects of C (2) methylation on thermal behavior and

interionic interactions in imidazolium-based ionic liquids with highly symmetric anions, *Applied Sciences* 8(7) (2018) 1043.

[30] S.K. Panja, H. Boumediene, M. Drai, D. Villemin, S. Bresson, Probing effect of weak H-bonding on conformational change in ionic liquid: Experimental and DFT studies, *Journal of Molecular Liquids* 266 (2018) 727-732.

[31] B. Haddad, A. Paolone, D.Villemin, J. F.Lohier, M.Drai, S.Bresson, , ... & E. H. Belarbi, para-Xylyl bis-1-methylimidazolium bis (trifluoromethanesulfonyl) imide: Synthesis, crystal structure, thermal stability, vibrational studies. *Journal of Molecular Liquids 260*(2018) 391-402.

[32]   S.K. Panja, B. Haddad, J. Kiefer, Clusters of the Ionic Liquid 1-Hydroxyethyl-3-methylimidazolium Picrate: From Theoretical Prediction in the Gas Phase to Experimental Evidence in the Solid State, *ChemPhysChem* 19(22) (2018) 3061-3068.

[33] Y. Liu, C. Ma, S. Men, Y. Jin, An investigation of trioctylmethylammonium ionic liquids by X-ray photoelectron spectroscopy: The cation-anion interaction, *Journal of Electron Spectroscopy and Related Phenomena* 223 (2018) 79-83.

[34] B. Haddad, S. A.Brandán, A. M.Amin, A. Paolone, D.Villemin, , & S.Bresson, Bidentate cation-anion   coordination   in   the   ionic   liquid   1-ethyl-3-methylimidazolium hexafluorophosphate supported by vibrational spectra and NBO, AIM and SQMFF calculations. *Journal of Molecular Structure* (2020) 128104.

[35] S.Zhang, J.Wang, X.Lu, & Q. Zhou, (Eds.). *Structures and interactions of ionic liquids* (Vol. 151). (2013) Springer.

[36] V. H. Paschoal, L. F. Faria, & M. C. Ribeiro, Vibrational spectroscopy of ionic liquids. *Chemical reviews*, *117*(10) (2017) 7053-7112.

[37] J. Kausteklis, V. Aleksa, M.A. Iramain, S.A. Brandán, Cation-anion interactions in 1-buthyl-3-methyl imidazolium nitrate ionic liquid and their effect on their structural and vibrational properties, *Journal of Molecular Structure* 1164 (2018) 1-14.

[38] J. Kausteklis, V. Aleksa, M.A. Iramain, S.A. Brandán, DFT study and vibrational assignment of 1-Butyl-3-methylimidazolium trifluoromethanesulfonate ionic liquid by using the FT-Raman spectrum, *Journal of Molecular Structure* 1175 (2019) 663-676.

[39] J. W. Sprague, J. G. Grasselli, , & W. M. Ritchey, The synthesis and infrared and nuclear magnetic resonance spectra of ammonium dicyanamide. *The Journal of Physical Chemistry 68*(2) (1964) 431-433.

[40] F.M. Vitucci, F. Trequattrini, O. Palumbo, J.B. Brubach, P. Roy, M.A. Navarra, S. Panero, A. Paolone, Stabilization of different conformers of bis (trifluoromethanesulfonyl) imide anion in ammonium-based ionic liquids at low temperatures, *The Journal of Physical Chemistry A* 118(38) (2014) 8758-8764.

[41] M.S. Miran, T. Yasuda, M.A.B.H. Susan, K. Dokko, M. Watanabe, Binary protic ionic liquid mixtures as a proton conductor: high fuel cell reaction activity and facile proton transport, *The Journal of Physical Chemistry C* 118(48) (2014) 27631-27639.

[42] T.A. Lima, V.H. Paschoal, L.F.O. Faria, M.C.C. Ribeiro, C. Giles, Comparing two tetraalkylammonium ionic liquids. I. Liquid phase structure, *The Journal of chemical physics* 144(22) (2016) 224504.

[43] L.F.O. Faria, J.R. Matos, M.C.C. Ribeiro, Thermal analysis and Raman spectra of different phases of the ionic liquid butyltrimethylammonium bis (trifluoromethylsulfonyl) imide, *The Journal of Physical Chemistry* B 116(30) (2012) 9238-9245.

[44] U. Domańska, R.J.T.J.o.P.C.B. Bogel-Łukasik, Physicochemical properties and solubility of alkyl-(2-hydroxyethyl)-dimethylammonium bromide, *The Journal of Physical Chemistry B* 109(24) (2005) 12124-12132.

[45] O. Palumbo, F.M. Vitucci, F. Trequattrini, A. Paolone, A study of the conformers of the N, N-diethyl-N-methyl-N-propylammonium ion by means of infrared spectroscopy and DFT calculations, *Vibrational Spectroscopy* 80 (2015) 11-16.

[46] S. Aparicio, M. Atilhan, M. Khraisheh, R. Alcalde, Study on hydroxylammonium-based ionic liquids. I. Characterization, *The Journal of Physical Chemistry B* 115(43) (2011) 12473-12486.

[47] E. Bodo, P. Postorino, S. Mangialardo, G. Piacente, F. Ramondo, F. Bosi, P. Ballirano, R. Caminiti, Structure of the molten salt methyl ammonium nitrate explored by experiments and theory, *The Journal of Physical Chemistry B* 115(45) (2011) 13149-13161.

[48] F. Capitani, C. Fasolato, S. Mangialardo, S. Signorelli, L. Gontrani, P. Postorino, Heterogeneity of propyl-ammonium nitrate solid phases obtained under high pressure, *Journal of Physics and Chemistry of Solids* 84 (2015) 13-16.

[49] T. Niemann, D. Zaitsau, A. Strate, A. Villinger, R. Ludwig, Cationic clustering influences the phase behaviour of ionic liquids, *Scientific reports* 8(1) (2018) 1-7.

[50] B. Haddad, A. Paolone, D. Villemin, M. Taqiyeddine, E.-h. Belarbi, S. Bresson, M. Rahmouni, N.R. Dhumal, H.J. Kim, J. Kiefer, Synthesis, conductivity, and vibrational spectroscopy of tetraphenylphosphonium bis (trifluoromethanesulfonyl) imide, *Journal of Molecular Structure* 1146 (2017) 203-212.

[51] A.B. Nielsen, A.J. Holder, *GaussView*, User´s Reference, GAUSSIAN, Inc.: Pittsburgh, PA, USA, 2000-2003.

[52] Gaussian 09, Revision A.02, M. J. Frisch, G. W. Trucks, H. B. Schlegel, G. E. Scuseria, M. A. Robb, J. R. Cheeseman, G. Scalmani, V. Barone, B. Mennucci, G. A. Petersson, H. Nakatsuji, M. Caricato, X. Li, H. P. Hratchian, A. F. Izmaylov, J. Bloino, G. Zheng, J. L. Sonnenberg, M. Hada, M. Ehara, K. Toyota, R. Fukuda, J. Hasegawa, M. Ishida, T. Nakajima, Y. Honda, O. Kitao, H. Nakai, T. Vreven, J. A. Montgomery, Jr., J. E. Peralta, F. Ogliaro, M. Bearpark, J. J. Heyd, E. Brothers, K. N. Kudin, V. N. Staroverov, R. Kobayashi, J. Normand, K. Raghavachari, A. Rendell, J. C. Burant, S. S. Iyengar, J. Tomasi, M. Cossi, N. Rega, J. M. Millam, M. Klene, J. E. Knox, J. B. Cross, V. Bakken, C. Adamo, J. Jaramillo, R. Gomperts, R. E. Stratmann, O. Yazyev, A. J. Austin, R. Cammi, C. Pomelli, J. W. Ochterski, R. L. Martin, K. Morokuma, V. G. Zakrzewski, G. A. Voth, P. Salvador, J. J. Dannenberg, S. Dapprich, A. D. Daniels, Ö. Farkas, J. B. Foresman, J. V. Ortiz, J. Cioslowski, and D. J. Fox, Gaussian, Inc., *Wallingford CT*, 2009.

[53] A.D. Becke, Density-functional exchange-energy approximation with correct asymptotic behavior, *Phys. Rev.* A38, 1988, 3098-3100.

[54] C. Lee, W. Yang, R.G. Parr, Development of the Colle-Salvetti correlation-energy formula into a functional of the electron density. *Phys. Rev.* B37, 1988, 785-789.

[55] B.H. Besler, K.M. Merz Jr, P.A. Kollman, Atomic charges derived from semiempirical methods, *J. Comp. Chem.* 1990, 11, 431-439.

[56] E.D. Glendening, J.K. Badenhoop, A. D. Reed, J. E. Carpenter, F. Weinhold, NBO 3.1; Theoretical Chemistry Institute, *University of Wisconsin; Madison*, WI, 1996.

[57] R.F.W. Bader, Atoms in Molecules, A Quantum Theory, Oxford University Press, Oxford, 1990, ISBN: 0198558651.

[58] F. Biegler-Köning, J. Schönbohm, D. Bayles. AIM2000; A Program to Analyze and Visualize Atoms in Molecules, *J. Comput. Chem.* 2001, 22, 545.

[59] P. Pulay, G. Fogarasi, G. Pongor, J.E. Boggs, A. Vargha, Combination of theoretical ab initio and experimental information to obtain reliable harmonic force constants. Scaled quantum mechanical (QM) force fields for glyoxal, acrolein, butadiene, formaldehyde, and ethylene. *J. Am. Chem. Soc.,* 1983, 105, 7073.

[60] G. Rauhut, P. Pulay, Transferable Scaling Factors for Density Functional Derived Vibrational Force Fields. *J. Phys. Chem.* 1995, 99, 3093-3100,

[61] T. Sundius, Scaling of ab-initio force fields by MOLVIB. *Vib. Spectrosc.* 2002, 29, 89-95.

[62] G. Keresztury, S. Holly, G. Besenyei, J. Varga, A.Y. Wang, J.R. Durig. Vibrational spectra of monothiocarbamates-II. IR and Raman spectra, vibrational assignment, conformational analysis and *ab initio* calculations of *S*-methyl-*N,N*-dimethylthiocarbamate *Spectrochim. Acta,* 1993, 49A, 2007-2026.

[63] D. Michalska, R. Wysokinski, The prediction of Raman spectra of platinum(II) anticancer drugs by density functional theory, *Chemical Physics Letters*, 2005, 403, 211-217.

[64] R. Ditchfield, Self-consistent perturbation theory of diamagnetism. I. A gage-invariant LCAO (linear combination of atomic orbitals) method for NMR chemical shifts, *Mol Phys.* 1974, 27, 714–722.

[65] P. Ugliengo, MOLDRAW Program, University of Torino, Dipartimento Chimica IFM, *Torino, Italy*, 1998.

[66] M. Boumediene, B. Haddad, A. Paolone, M. Drai, D. Villemin, M. Rahmouni, S. Bresson, O. Abbas, Synthesis, thermal stability, vibrational spectra and conformational studies of novel dicationic meta-xylyl linked bis-1-methylimidazolium ionic liquids, *Journal of Molecular Structure* 1186 (2019) 68-79.

[67] B. Haddad, A.Paolone, M. Drai, M. Boumediene, D. Villemin, E. H. Belarbi, , ... & O. Abbas, Para-xylyl linked bis-imidazolium ionic liquids: A study of the conformers of the cation and of the anion-cation hydrogen bonding. *Journal of Molecular Structure 1175* (2019) 175-184.

[68] D. Luo, J. Huang, Y. Zhang, H. Liu, P. Hu, Highly efficient separation and extraction of vanadium from a multi-impurity leachate of vanadium shale using tri-n-octylmethylammonium chloride, *Separation and Purification Technology* 230 (2020) 115842.

[69] D. Luo, J. Huang, Y. Zhang, H. Liu, P.Hu, Efficient and environment-friendly vanadium (V) extraction from vanadium shale leachate using tri-n-octylmethylammonium chloride *Sep. Purif. Technol*. **237** 2020 116482.

[70] M. Drai, A. Mostefai, A. Paolone, B. Haddad, E. Belarbi, D. Villemin, S. Bresson, O. Abbas, Y. Chaker, M. Rahmouni, Synthesis, experimental and theoretical vibrational studies of 1-methyl and 1, 2-dimethyl, 3-propyl imidazolium bis (trifluoromethanesulfonyl) imide, *Journal of Chemical Sciences* 129(6) (2017) 707-719.

[71] E. Pigorsch, Spectroscopic characterisation of cationic quaternary ammonium starches, Starch-Stärke 61(3-4) (2009) 129-138.

[72] R. A. Rudyk, M.A. Checa, C. A. N. Catalán, S.A. Brandán, Structural, FT-IR, FT-Raman and ECD studies on the free base, cationic and hydrobromide species of scopolamine alkaloid, *Journal of Molecular Structure* 1180 (2019) 603-617.

[73] S.A. Brandán, Why morphine is a molecule chemically powerful. Their comparison with cocaine, *Indian Journal of Applied Research* 7(7) (2017) 511-528.

[74] S.A. Brandán, Understanding the potency of heroin against to morphine and cocaine, IJSRM, International *Journal of Science And Research Methodology* 12(2) (2018) 97-140.